Effects of organic modifiers on the colloidal stability of TiO_2 nanoparticles. A methodological approach for NPs categorization by multivariate statistical analysis

Andrea Brunelli,[‡a] Elena Badetti,[‡*a] Gianpietro Basei,[a] Francesca Caterina Izzo,[a] Danail Hristozov,[b] Antonio Marcomini*[a]

[a]DAIS - Department of Environmental Sciences, Informatics and Statistics, University Ca' Foscari of Venice, Via Torino 155, 30170 Venice Mestre, Italy.
[b]Greendecision Srl., Via delle industrie 21/8, 30175 Venice Marghera, Italy
‡These authors contributed equally.
*Corresponding author.
E-mail: elena.badetti@unive.it, marcom@unive.it

Abstract

The considerable diversity and complexity of manufactured nanoparticles (NPs) have made their regulatory safety assessment challenging due to the need for excessive testing. Therefore, it is relevant to derive physicochemical and structural descriptors for *in silico* modelling that can help to develop strategies for "Safety by Design" (SbD) in the early stages of product development. This paper aims at informing such strategies by studying how surface modification by means of attaching organic ligands can affect the colloidal stability of nanoscale TiO_2 in different environmental media with changing electrolyte concentrations and pH levels. The functionalization was performed by using four catecholate derivatives (catechol, 3,4-dihydroxybenzaldehyde, 3,4-dihydroxybenzoic acid, dopamine hydrochloride), salicylic acid and polyethylene glycol (PEG) polymer. Surface charge, hydrodynamic diameter and sedimentation velocity were measured to assess the colloidal stability of each of the dispersions. Then, statistical clustering techniques and Principal Component Analysis (PCA) were applied to the obtained experimental data in order to identify physicochemical descriptors and classes of stability, which were used to classify the investigated surface modifications. In conclusion, the proposed approach, combining experimental results from simple and fast techniques with multivariate statistical methods has proven to be useful for supporting nanomaterials categorization for the purpose of developing SbD strategies.

Keywords: Titanium dioxide nanoparticles; Organic ligands; Colloidal stability, Categorization, pH; Ionic strength; Principal component analysis.

1. Introduction

Manufactured nanoparticles (NPs) are being used in a wide variety of industrial applications and consumer products.[1] However, the high heterogeneity of novel nanoforms released on the market has made their safety assessment very demanding in terms of testing. To reduce this high regulatory burden of proof of the nanotechnology industry it has been suggested to employ *in silico* modelling as well as grouping and read-across approaches to enable safety by design (SbD) strategies that target the early stages of product innovation.[2] This is challenging as the physicochemical identity of the nanomaterials can be easily affected upon contact with any biological, environmental or industrial dispersion media. The most frequently observed phenomena are aggregation and/or agglomeration of the NPs in the medium as a result of e.g. its chemical composition, pH, ionic strength, dissolved concentration of oxygen and sulphide, light, suspended particle matter, or content of natural organic matter. This leads to changes in the size distribution, shape, surface area and charge of the NPs, all of which are properties that directly determine their industrial functionality, exposure potential, and/or adverse (eco)toxicological effects. This poses challenges not only to the safety assessment of these materials, but also to the reproducibility of product performance, which are major barriers to nanotechnology innovation.

Therefore, understanding how the interactions between NPs and the surrounding medium can alter their colloidal dispersion stability is essential not only to predicting their risks, but also to developing SbD strategies[3] that can prevent these risks early in the R&D process.[4] Specifically, it can help to derive descriptors for *in silico* and materials modelling of both properties and effects and to design *in vitro* (eco)toxicological tests as part of Intelligent Testing Strategies that aim at reducing testing costs and the use of experimental animals. It can also help in the better interpretation of the modelling/testing results[5] to derive criteria and guiding principles for grouping and/or read-across and for classification according to regulatory requirements and industrial product quality criteria.

To contribute to the above priorities, the goal of this paper is to investigate the influence of surface modification on the extrinsic properties of the NPs, defined as the "characteristics that are linked to the material's functionality in its environment".[6] Our case study is nanoscale titanium dioxide (TiO_2), which was selected due to its widespread use in many consumer products, very low solubility, and surface which can be easily modified.[7,8] Specifically, we used different modifying substances: catecholate derivatives (i.e. catechol, 3,4-dihydroxybenzaldehyde, 3,4-dihydroxybenzoic acid, dopamine hydrochloride), salicylic acid (SAL), and polyethylene glycol (PEG), exploiting the optimal geometry of these ligands to get covalently linked to the NPs' surfaces. The catecholate-type ligands were chosen because of their versatile chemistry, which allowed easier attachment of different functional groups, leading to new optically active nanomaterials[9] as well as to fundamental building blocks for the synthesis of more complex architectures.[10–12] Salicylic acid was chosen for its similarity to catechols in terms of structure, functional groups, and way of binding to TiO_2 surface. The surface modification with PEG was performed because polymeric coatings are considered one of the main approaches to effectively control physicochemical properties such as size, surface charge and solubility, all of which are parameters known to determine the toxicokinetics and toxicity of nanomaterials.[13]

Once the surfaces of the materials were functionalized, their colloidal stability was assessed in different dispersion media (with different electrolyte concentrations and pH levels) by combining Electrophoretic Light Scattering (ELS), Dynamic Light Scattering (DLS) and Centrifugal Separation Analysis (CSA) techniques. The obtained data were analysed through statistical clustering methods and Principal Component Analysis (PCA),[14] which had been previously applied for classification of nanomaterials[15,16] as well as for quality assessment of nano-based dispersions.[17] This led to understanding which combinations of intrinsic and extrinsic properties affected the obtained classification into high-, moderate- and low-stability dispersions. These descriptors can be used for *in silico* modelling of colloidal stability, while the classification methodology and results can be useful for developing SbD strategies.

2. Materials and methods

2.1 Case-study nanomaterial and other reagents

The inorganic Aeroxide® P25 titanium dioxide nanopowder was purchased from Evonik Degussa (Germany). P25 powder (declared average particle size: 21 nm) is a mixture of approx. 80% anatase and 20% rutile, with 99.5% purity, 50 ± 15 m^2/g as surface area, and a bulk density of 3.8 g/cm^3. Catechol (CAT), 3,4-dihydroxybenzaldehyde (CHO), 3,4-dihydroxybenzoic acid (COOH), dopamine hydrochloride (DOP), salicylic acid (SAL), polyethylene glycol (PEG, Mv 100000) and all the other chemicals were of the highest purity available and were used without further purification (Sigma Aldrich, St. Louis, MI, USA). Ethanol (Romil Ltd, Cambridge, UK), deionized water (resistivity 18.2 MΩ/cm), NaCl (1 and 10 mM) solutions, Artificial Fresh Water (AFW, 2 mM ionic strength) and Artificial Marine Water (AMW, 630 mM ionic strength) were used as dispersant media. AFW and AMW were prepared according to standardized protocols.[18,19]

2.2 Synthesis of surface modified TiO_2 nanoparticles

According to different recommendations and guidelines for NPs dispersion procedures described in the literature[20,21] an ethanolic suspension of P25 NPs (2 g/L) was sonicated with an ultrasonic probe (UP-200S Hielscher Ultrasonics GmbH, Germany) in an ice bath, delivering a power of 200 W for 15

min using a pulsed 80% mode. The surface modification of P25 NPs was achieved by the addition of each surface-active ligand up to concentrations highest than the theoretically required to cover all surface sites: catecholate type ligands (20 mM), salicylic acid (20 mM) and PEG (2 mM), all dissolved in EtOH. The formation of modified P25 NPs dispersions was obtained by mixing 25 mL of each ligand solution to 100 mL of P25 NPs suspension, which was sonicated in an ice bath by ultrasonic probe over 1h and then it was consequently let stirring overnight at room temperature. Afterwards, each suspension was centrifuged until the P25 NPs settled completely. The supernatant was removed, and the particles were washed three times by adding 10 mL of EtOH to remove the possible excess of unlinked ligand, followed by ultra-sonication and finally by centrifugation of the new suspension until the complete settling of the NPs. After the last washing step, the NPs were dried leading to powders with different colours, depending on the functionalization performed (S1). Schematics of the functionalized nanomaterials is reported in Figure 1.

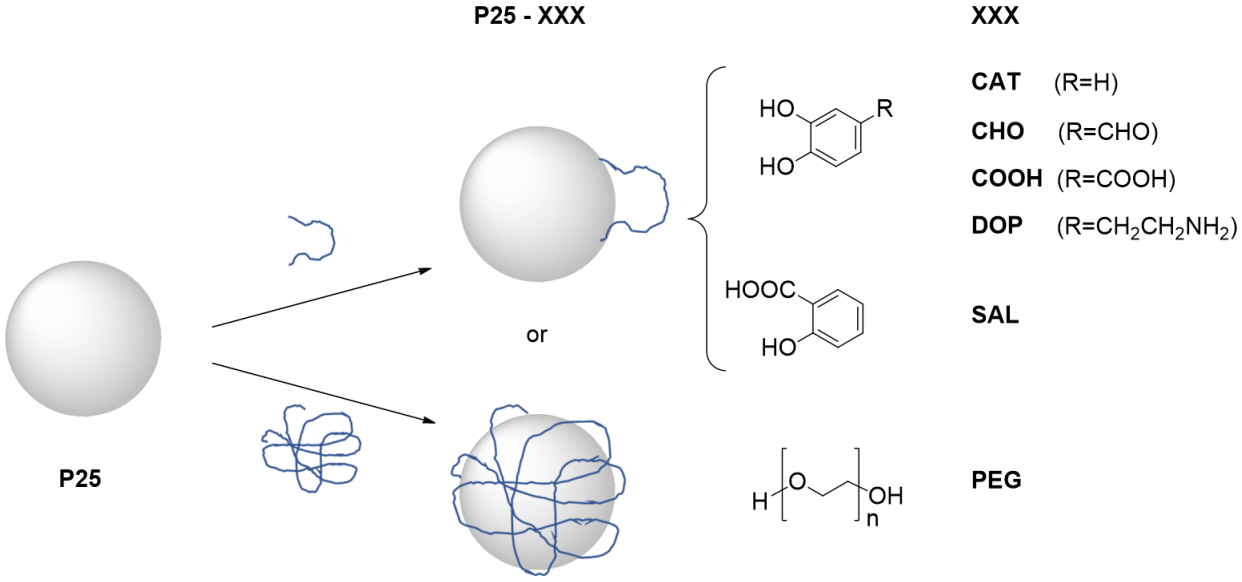

Figure 1. Schematics of P25 NPs surface functionalization with the selected organic ligands.

2.3 Physico-chemical characterization

The physico-chemical characterization on the dry powders was performed by means of Fourier-Transformed Infrared spectroscopy (FTIR), Thermo-Gravimetric Analysis (TGA) and Differential Scanning Calorimetry (DSC).

In detail, FTIR analysis was performed with a Thermo Nicolet Nexus 670 FT-IR spectrophotometer equipped with a Smart Orbit Single Reflection Diamond ATR (Attenuated Total Reflection) accessory, from 4000 to 400 cm^{-1} for 64 scans with 4 cm^{-1} resolution. FTIR data were elaborated with Omnic 8.0 and Origin 8.0 softwares.

TGA and DSC were performed simultaneously using a Netzsch 409/C apparatus. The temperature program used was set up experimentally from 30 °C, 10 °C min^{-1} to 600 °C. The TG-DSC analyses were performed in air and the instrument was purged with N_2 at a flow rate of 40 mL/min. The samples masses ranged between 4 and 8 mg; samples were put in a platinum crucible and alumina was used for the internal calibration. Three replicates were performed for each sample. Data were collected with STA Netzsch software and then elaborated with Origin 8.0 software.

The colloidal characterization was performed by means of Dynamic Light Scattering (DLS), Electrophoretic Light Scattering (ELS) and Centrifugal Separation Analysis (CSA), re-dispersing the NPs at 50 mg/L in the following media: NaCl solutions, deionized water, AFW and AMW. This concentration was selected to obtain the optimal signal-to-noise ratio during the analysis. Before performing the colloidal characterization, each suspension was probe sonicated in an ice bath at 200 W for 15 min, pulsed 80% mode.

In detail, DLS and ELS were performed by means of the multi-angle Nicomp ZLS Z3000 (Particle Sizing System, Port Richey, FL, USA). The hydrodynamic diameter was measured with an optical fiber set at 90° scattering angle (W=25 mW and λ=639 nm) over at least 6 min at room temperature. Surface charge of the electric double layer of each sample was determined in two different electrolyte solutions (1 and 10 mM NaCl) in the pH 2-10 range, applying a 5 V electric field to obtain zeta-potential (Z-pot) values and measurements were taken after pre-equilibration of each sample for 30 min. NaCl was chosen as electrolyte for Z-pot measurements due to its inertia toward TiO_2,[22] which allowed to study the role of the different modifiers in the stabilization without altering the main structure of P25 NPs. Generally, Z-pot values of ±30 mV indicate a stable colloidal dispersion[22,23] and the isoelectric point (IEP), defined as the pH of zero net charge, represents the point of maximum instability. However, in the evaluation of colloidal stability it is important to consider that Z-pot gives information only on the electrostatic repulsive forces, without providing any insights on the attractive Van der Waals forces.[24–26]

Centrifugal Separation Analysis (CSA) was employed to assess dispersion stability of NPs in terms of sedimentation velocity. This method was already successfully applied to calculate the sedimentation kinetics of TiO_2 NPs and multi-walled carbon nanotubes[15,27] as well as to gather information on the sedimentation velocity distribution of CuO NPs in both environmental and biological media.[4] In detail, sedimentation velocity was determined through Centrifugal Separation Analysis (CSA), by using the Multiwavelength Dispersion Analyzer LUMiSizer® 651. The transmission profiles obtained by CSA represent the transmittance values over the length of the cuvette containing the sample. Particles migration due to centrifugal force results in a variation of the local particle concentration and, correspondingly, local and temporal variations of transmission occur.[28] The separation of different components in dispersion was achieved at 3000 Rotation Per Minute (RPM), which corresponds to a Relative Centrifugal Force (RCF) of 1207 at 120 mm far from the rotor of the centrifuge. Sedimentation velocity data were calculated from the transmittance values obtained setting the wavelength of the transmitted light at 470 nm and collecting the transmittance (%) over time at three different positions (115, 120 and 125 mm far from the rotor) over the length of the cuvette. The runtime of each analysis (i.e. 50 min) was chosen according to the lowest time needed to reach the plateau, i.e. the maximum transmittance values, indicating the complete sedimentation of NPs. The linear dependency between RCF and sedimentation velocity allowed to extrapolate sedimentation velocity data at gravity by dividing the results for the RCF applied.

Hydrodynamic diameter, surface charge and sedimentation velocity were measured in triplicate and results are expressed as average for DLS/ELS and as median for CSA.

2.3 Clustering and Principal Component Analysis (PCA)

Statistical analysis was carried out using R language. Hierarchical Clustering (HC) was performed using *hclust* function, k-Means (KM) was performed using *kmeans* function, and Principal Component Analysis (PCA) was performed using *prcomp* function, all included in the *stats* built-in package.[29] Fuzzy c-Means (FCM) was provided by the *cmeans* function from the *e1071* package,[30] and Nearest Neighbor for class prediction was carried out by means of the *knn* function from the *class* package.[31]

The experimental data obtained from the ELS, DLS and CSA techniques in NaCl solutions at different pH levels were statistically analysed to categorize the different dispersions into stability classes (i.e. high-, moderate- and low-stability classes). The identification of patterns without any *a priori* knowledge on data categorization was achieved by cluster analysis. Specifically, after data standardization (i.e. subtracting the mean and dividing by standard deviation of each descriptor), three different clustering algorithms (HC, KM and FCM) were applied to automatically derive three subsets of data sharing similarities among descriptors. More details on cluster analysis are reported in the SI.

The resulting clusters were labelled according to CSA values: cluster containing the sample with the highest CSA values was labeled as "low stability", cluster containing the sample with the lowest CSA values was labeled as "high stability", and "moderate stability" was the third cluster in between. By using DLS or ELS values to label the clusters instead of CSA, the same labeling was obtained. In addition to these three algorithms, a voting-based consensus clustering (CONS) was employed[32] to obtain a single classification method which included the information achieved from HC, KM and

FCM clustering techniques. Specifically, a voting system was applied as follows: for each clustering technique, 1 was assigned if the sample resulted in “low stability” class, 2 if sample was included in “moderate stability” class and 3 if it was in “high stability” class. Then, votes were averaged and the consensus clustering classified stability of each entry as "low" if average was lower than 1.5, "high" if it was higher than 2.5, and "moderate" in other cases.

Afterwards, a comparison of the classifications provided by each clustering technique was performed using the Adjusted Rand Index (ARI),[33] a widely used measure of agreement between two cluster results.[34,35] ARI is equal to 0 in case of two random partitions, and 1 in case of perfect agreement. ARI can also be negative, meaning that agreement is worse than expected as random.

In the case of samples dispersed in DW, AFW and AMW, in which ELS measurement were not reliable because of the lack or too high concentration of electrolytes in solution, another approach was used. The clustering algorithms previously described were used considering only DLS and CSA data, and the reliability of the procedure was confirmed by comparing the consensus clustering of these results with those obtained using the three techniques. Standardization of new data was performed by subtracting the same mean and dividing by the same standard deviation of each descriptor previously computed.

Then, the stability classes of the different dispersions were predicted using a Nearest Neighbor classifier for each clustering technique. In the case of HC, each data was assigned to the stability class of the closest element of the previous dataset, while by applying KM and FCM algorithms, data were assigned considering the closest centroids. The outcomes were merged following the consensus clustering definition in each of the three stability classes.

Finally, Principal Component Analysis (PCA) was used to reduce dimensionality of data space, highlighting data assignment from the results obtained by cluster analysis.

3. Results and discussion

3.1 Binding of organic ligands to P25 NPs surface

The coating of P25 NPs by chemisorption of the ligands selected was investigated by ATR-FTIR and TGA-DSC analysis.

The ATR-FTIR spectra of catechol free and adsorbed on P25 NPs are displayed in Fig. 2, as a zoom-in image of the wavelength region between 1800-1000 cm^{-1}. The main bands of free catechol (Fig. 2a) are the following: stretching vibration of the aromatic ring ν(C-C)/ν(C=C) at 1618, 1600, 1512, 1467 cm^{-1} and stretching of phenolic group ν(C-OH) at 1278, 1254 and 1237 cm^{-1}, while the bending vibrations of the phenolic group δ(C-OH) occur at 1360, 1183, 1163 and the bending δ(C-H) at 1093, 1039 cm^{-1}. The adsorption of catechol onto P25 NPs (Fig. 2b) led to relevant changes in ATR-FTIR spectrum: a loss of the hyperfine structure of bending δ(C-OH) vibration in the region below 1200 cm^{-1} was observed, the bands at 1360 and 1183 cm^{-1} disappeared and a very weak feature centred at 1327 cm^{-1} appeared. The band of stretching ν(C-OH) vibrations merged to one broad band centred at 1263 cm^{-1}. Such signals are assigned to stretching and bending vibrations of phenolic groups which participated in the complex formation with Ti surface atoms. Moreover, the stretching of the aromatic ring in the region above 1400 cm^{-1} was also affected by the binding to P25 NPs, showing a single band at 1484 cm^{-1}. According to the literature,[9] the observed signals suggested that catechol is bound at the P25 NPs surface. Moreover, ATR-FTIR spectrum of P25 NPs did not show any bands in 1800-1000 cm^{-1} region, but only the typical absorption band below 700 cm^{-1} due to the stretching of anatase and rutile TiO_2 (Ti–O–Ti) (Fig. S2).[36]

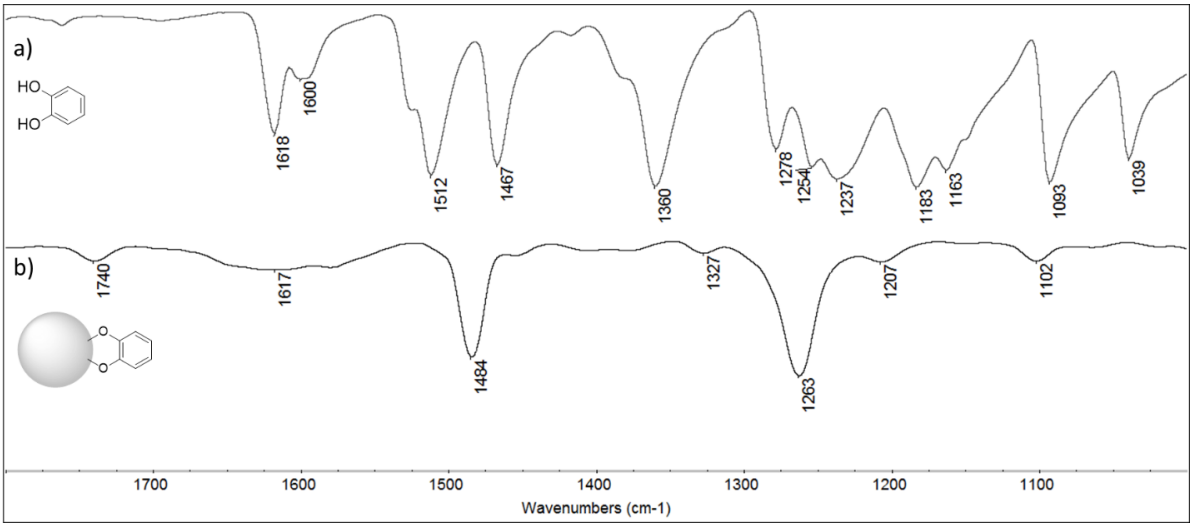

Figure 2. ATR-FTIR spectra of (a) free catechol and (b) P25-CAT NPs in the region between 1800 and 1000 cm^{-1}.

The ATR-FTIR spectra of 3,4-dihydroxybenzaldehyde (CHO), 3,4-dihydroxybenzoic acid (COOH) and dopamine hydrochloride (DOP) adsorbed on P25 NPs surface are reported in Fig. S3-S5. According to the literature, they showed the same way of ligand binding observed for catechol.[9] Moreover, the characteristic signals corresponding to the carboxyl group still appeared in the ATR-FTIR spectra of P25-COOH (stretching absorptions at 1695 and 1606 cm^{-1}) and P25-CHO (stretching band at 1674 cm^{-1}), indicating that these groups are not involved in the formation of the complexes. In the same way, a strong band corresponding to the amine of P25-DOP was observed at 1630 cm^{-1}. As far as salicylic acid, according to Jankovic et al.,[37] both phenolic and carboxylic groups are involved in the chelation of titanium atoms (Fig. S6) since the bands in the region between 1700 and 1560 cm^{-1} merged to one broad band centred at around 1600 cm^{-1}. Finally, ATR-FTIR spectra of P25 NPs functionalized with PEG polymer (Fig. S7) showed a strong absorption at around 1100 cm^{-1} corresponding to ether linkage (C-O-C bonds),[38,39] while the signals corresponding to -OH groups appeared very broad, indicating as these groups participated to the bonds formation. The overall results indicated the formation of the desired complexes and proved, for catecholate and salicylate ligands, the most likely formation of bidentate bridging complexes.

Thermal analysis of pristine and modified P25 NPs, carried out in the 30-600°C temperature range, was performed to estimate the NPs surface coverage rate for each ligand (Figure 3 and S8-10). TGA of pristine did not show any mass loss in the temperature range investigated, confirming the purity of the starting material already observed by FT-IR analysis. In detail, no organic components or water were adsorbed on pristine NPs surface which resulted to be composed only by anatase and rutile. As far as functionalized P25 NPs, a mass loss of around 3% was observed for NPs functionalized with CAT, COOH and DOP ligands, around 6% for CHO and SAL ligands up to 8% for P25-PEG. DSC analysis finally confirmed the chemisorption of the ligands, showing the exo-thermal processes occurring approximatively between 200 and 400 °C, related to the decomposition of the attached organic fraction.

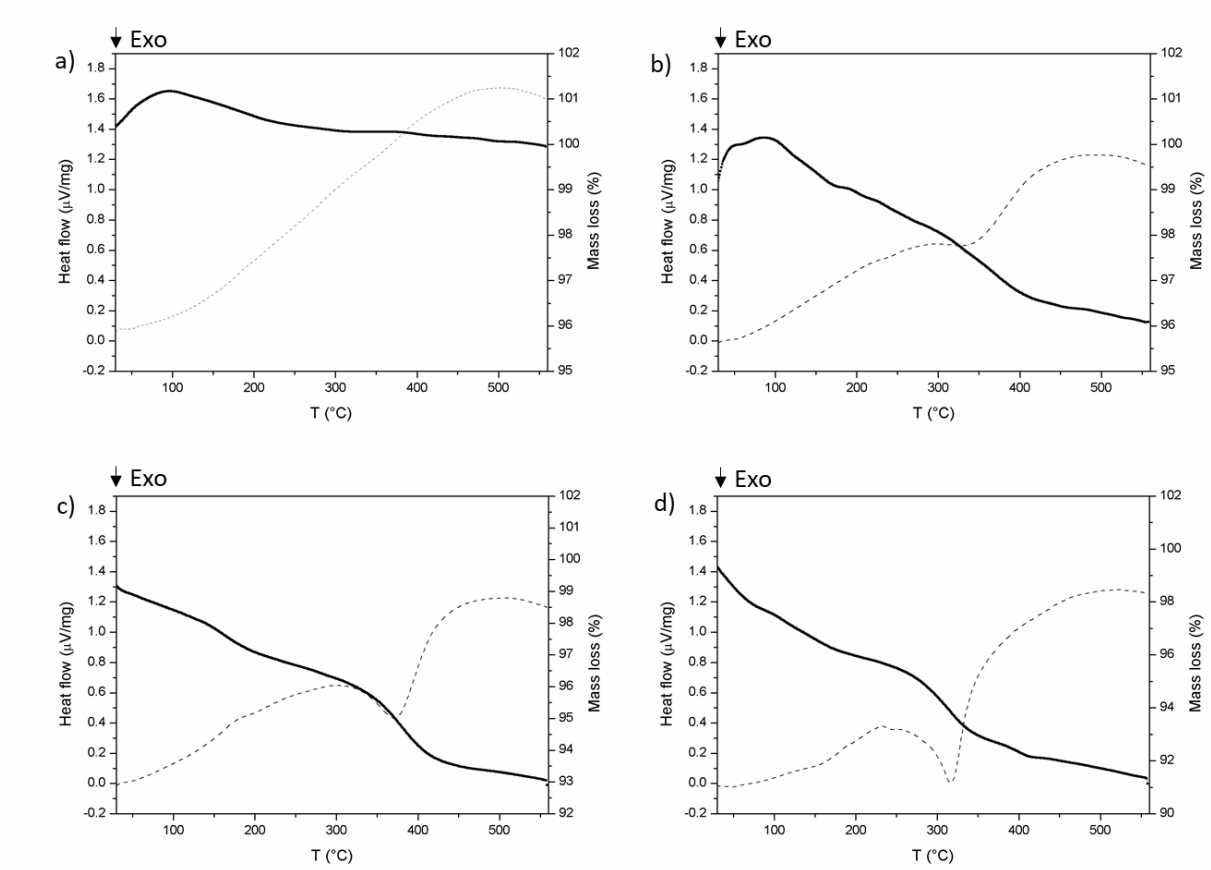

Figure 3. TG-DSC curves of a) P25 NPs, b) P25-CAT, c) P25-SAL, d) P25-PEG in the range of 30-600 °C. TG curve (solid line), DSC curve (dash line).

3.2 Colloidal stability assessment as a function of electrolyte concentration and pH

The colloidal stability of pristine and functionalized P25 NPs was initially investigated as a function of 2-10 pH range at 1 and 10 mM NaCl electrolyte concentrations, by combining ELS, DLS and CSA techniques. The overall results concerning zeta-potential, hydrodynamic diameter and sedimentation velocity of the different NPs were reported in Tables S1-S3 and graphically represented in Fig. 4.

3.2.1 Electrophoretic Light Scattering (ELS)

A titration curve of Z-pot vs pH was obtained to determine the IEP for each NPs dispersion (Fig. 4). According to the literature, the IEP of pristine P25 NPs was calculated around pH 6.[40,41] P25-DOP showed an IEP very close to that calculated for pristine while, for the other TiO_2 NPs functionalized with catecholate-type ligands and for P25-PEG, the IEP was around pH 5. Finally, the IEP of P25-SAL was determined at pH 7. In general, Z-pot moved from positive values in the acid pH region before the IEP, to negative values in the region after the IEP, regardless of the surface functionalization. Both pristine P25 and all the functionalized NPs led to Z-pot values between ± 30 mV. The titration curves displayed in Fig. 4 showed, for each compound, very similar values of Z-pot vs pH at the two NaCl concentration studied. The independence between IS and surface charge is consistent with data reported in literature[22] and can be ascribed to the electrolyte nature of the salt investigated. As commented before, NaCl is inert for TiO_2 and no specific adsorption of Na^+ and Cl^- by titania NPs occurred. However, while considering only Z-pot results the ionic strength had no influence on the colloidal stability, a different behaviour was observed from DLS and CSA results.

3.2.2 Dynamic Light Scattering (DLS)

Dynamic Light Scattering (DLS) was employed as one of the most common and easy-to-use light scattering techniques to determine the hydrodynamic diameter of NPs dispersions. According to the classical Derjaguin-Landau-Verwey-Overbeek (DLVO) theory, to an increase of the ionic strength corresponds a raise of the hydrodynamic particles size of NPs (i.e. aggregation), inducing a destabilization of the colloidal suspension.[42] This phenomenon, differently from the trend observed for ELS results, was confirmed for all the dispersions tested along the entire pH range investigated, increasing up to four times the hydrodynamic size from 1 to 10 mM NaCl (Fig. 4). Concerning the effect of pH, P25 pristine dispersions within the acid pH range (from 2 to 4) displayed hydrodynamic particles size < 700 nm. An increase of the hydrodynamic diameter from 800 to 1320 nm was observed at pH 6, which corresponds to the IEP, and at basic pH (8-10), reaching 1470 nm size. Concerning the functionalized NPs, different behaviours were observed depending on the functional group attached on the NPs surface. As depicted in Fig. 4, hydrodynamic diameters of P25-CAT and P25-DOP were more affected by electrolyte concentration than by pH (increasing approximatively from 500 nm at 1 mM NaCl to 1000 nm at 10 mM NaCl). As far as P25-CHO and P25-SAL, the main parameter affecting hydrodynamic particles size was pH, showing an opposite trend between the two samples. The lowest hydrodynamic particles size values (< 550 nm) were measured at pH ≥ 6 for P25-CHO while an increment of size around 1000 nm was observed under acid conditions. On the other hand, P25-SAL reached the highest size values around 1400 nm at pH ≥ 6 and lowest hydrodynamic size at around 500 nm in the acid pH range (2-4). As expected, the coating of P25 with PEG polymer led to NP dispersions not significantly influenced by the two parameters investigated (electrolyte concentration and pH), showing an average of hydrodynamic particles size always around 1000 nm. Finally, P25-COOH showed a hydrodynamic diameter slightly influenced by electrolyte concentration and even less by pH, showing values < 500 nm at 1mM NaCl and < 900 nm at the highest electrolyte concentration.

3.2.3 Centrifugal Separation Analysis (CSA)

CSA technique allows to compare different colloidal dispersions and to establish a relative stability ranking under specific experimental conditions. In general, at increasing sedimentation velocity corresponds a decrease of dispersion stability. As far as pristine P25 NPs, the sedimentation velocity of NPs dispersions was mainly affected by pH values rather than by electrolyte concentration (Fig. 4). Low sedimentation velocity values < 0.10 μm/s were collected in the acid pH range from 2 to 4, while values increased up to 0.30 μm/s at pH ≥ 6. On the contrary, as already observed from DLS results, sedimentation velocity values of P25-CAT and P25-DOP were mainly driven by electrolyte concentration, in fact they increased from 0.03 μm/s to 0.22 μm/s. According to DLS data, a strong effect of pH on sedimentation velocity values was clearly observed for P25-CHO and P25-SAL. P25-CHO showed the lowest values at basic pH, especially at 1 mM NaCl (< 0.04 μm/s), while P25-SAL displayed analogous sedimentation velocity values in the acid pH range (2-4). Similar to the trend observed from DLS results, P25-PEG sedimentation velocities were quite constant along the whole pH range investigated (0.15-0.23 μm/s) and P25-COOH presented very low values (all < 0.15 μm/s) at each pH examined, also at the highest electrolyte concentration. As a result, the overall CSA and DLS data were in good agreement to assess colloidal stability for almost all the samples analysed. Nevertheless, although to an increase of the sedimentation velocity corresponded an increase of the hydrodynamic particles size and vice versa, a direct proportionality between the results obtained by the two techniques was not observed. This finding was expected since the two techniques are based on different forces driving particle-migration: diffusion for DLS and centrifugal forces for CSA. Moreover, DLS is more sensitive to the scattering signal of larger particles size and often masks the signal of the smaller counter parts.[17]

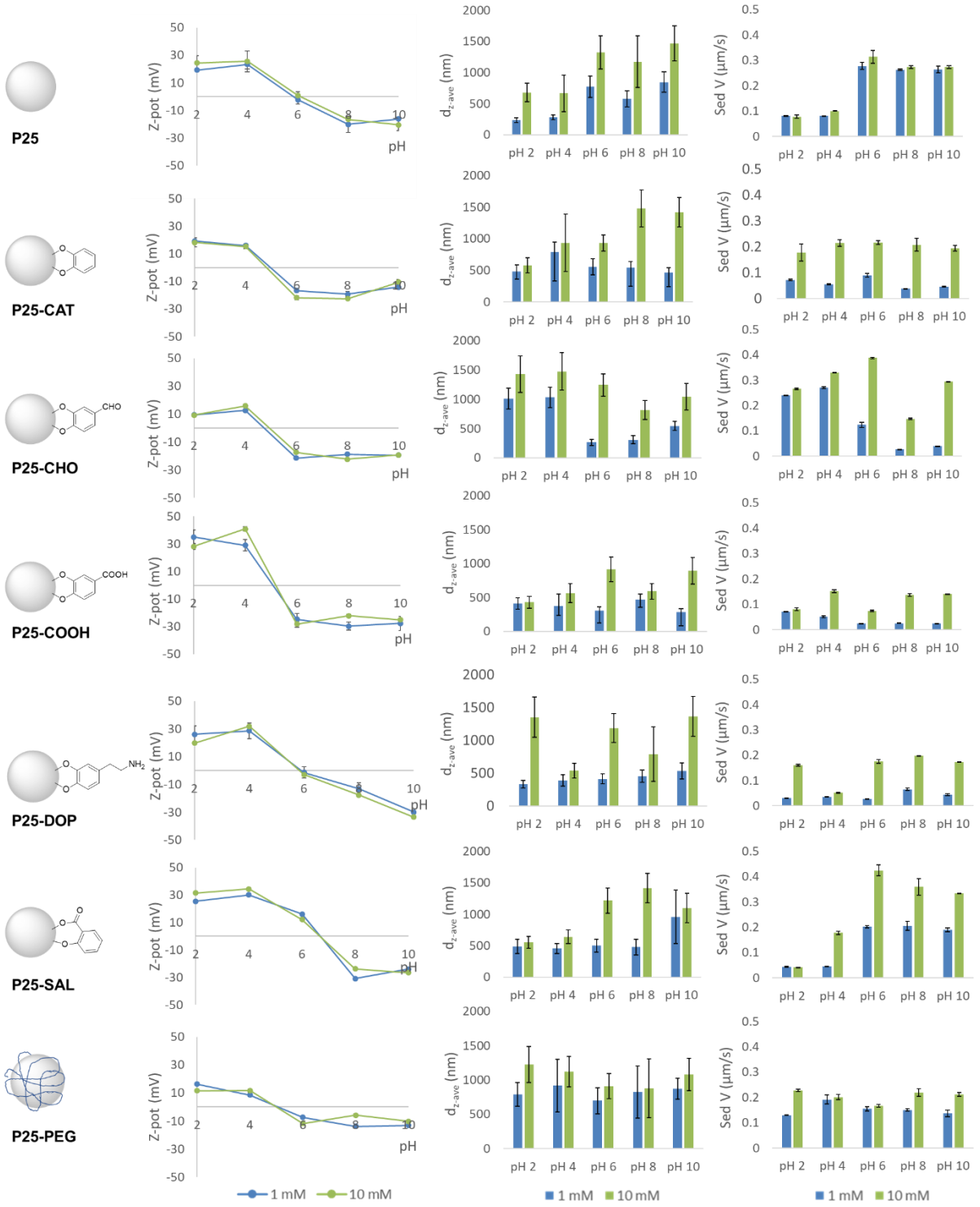

Figure 4. Zeta-potential (Z-pot), hydrodynamic diameter ($d_{z\text{-}ave}$) and sedimentation velocity (Sed V) data of pristine and functionalized P25 NPs dispersed in 1 and 10 mM NaCl solution in the pH range from 2 to 10.

3.2.4 Stability categorization by statistical analysis

The experimental data from ELS, DLS and CSA techniques (Tables S1-S3) were statistically analysed by clustering and PCA to categorize the different dispersions into relative stability classes as a function of the investigated intrinsic and extrinsic physicochemical parameters. NPs were clustered into three main categories, which were labelled as high, moderate, and low stability classes. The three clusters algorithms applied (i.e. Hierarchical clustering (HC), K-means (KM) and Fuzzy c-Means (FCM)), agreed in arranging data as follows: samples with high CSA and DLS values and low ELS absolute values were grouped together, as well as samples with high ELS absolute values and low CSA and DLS values.

The obtained results are reported in Table S4, together with data from the voting-based Consensus clustering (CONS) performed to merge all the information achieved by the three clustering techniques. In addition, the Adjusted Rand Index (ARI) was used to assess the similarity among the four different clustering algorithms and the results are reported in Table S5, showing a good agreement among the statistical techniques.

The categorization obtained by Consensus clustering is displayed by PCA in S11 and it was split for clarity into three different PCA plots with respect to pH: (I) acid pH range between 2 and 4 (Fig. 5a); (II) around the isoelectric point, i.e. pH 6 (Fig. 5b); (III) basic pH range between 8 and 10 (Fig. 5c). The ellipses depicted in each stability region represented the 68% confidence interval of data, under the reasonable assumption of normal distribution. In general, almost the same direction for the arrows corresponding to DLS and CSA data was observed (Fig. 5 and S11), showing a high correlation between these two techniques. Both hydrodynamic particles size and sedimentation velocity values increased along with the direction of the arrows, indicating a decrease of the dispersion stability. On the contrary, zeta-potential data considered as absolute values, showed an increase of the stability. A change of ELS arrow orientation along the pH scale was observed moving from the acid to the basic pH. In fact, the ELS arrow became practically orthogonal to DLS and CSA arrows, indicating an increased contribution of zeta-potential to PC2 at basic pH. In detail, as far as strong acid pH (2-4), the first principal component PC1 accounted for 80.8% of the whole variance while PC2 accounted for 13.9% of the total variability (Fig. 5a). This translates in a quite good agreement among the three analytical techniques under strong acid conditions. On the other hand, PC1 of pH 6 plot (Fig. 5b) accounted for 63.9% of the total variance and the second accounted for 27.7%. Finally, PC1 from the basic pH (8-10) plot (Fig. 5c) accounted for slightly more than half, i.e. 57.7%, and the second for roughly one third, i.e. 32.3%, indicating the same contribution from each technique to the total variability. The increment in the contribution of PC2 from acid to basic pH was mainly ascribed to ELS.

An increase of surface functionalized NPs colloidal stability with respect to pristine was observed in PCA plots from pH 6 to 10 (i.e. Fig. 5b-5c). As expected from literature,[43] pristine dispersions already resulted highly stable under acid conditions (Fig. 5a), along with all the P25-COOH and P25-SAL dispersions tested. A possible explanation of the high stability of these two functionalized NPs can be ascribed to the carboxylic group. In fact, as far as P25-COOH, -COOH group was not involved in the modification of P25 surface, as highlighted by FTIR spectrum (Fig. S4). Moreover, in the case of P25-SAL, the protonation of the carboxylic group attached on titanium might occur under strong acid conditions, leading to a monodentate conformation and to the free COOH group. On the other hand, P25-CAT and P25-PEG were mainly located in the moderate stability class while the less stable dispersions were represented by P25-CHO. P25-DOP was an exception, resulting highly stable at pH 4, but varying its stability class at pH 2 depending on the electrolyte concentration. Taking into account the results at pH 6 (Fig. 5b), P25-COOH, P25-CHO and P25-CAT were categorized within the high-stability class. However, while P25-COOH was highly stable regardless the NaCl concentration, P25-CHO and P25-CAT moved respectively to the low- and moderate-stability classes at 10 mM NaCl solutions. The sensitivity to the salt concentrations was also observed for P25-SAL, which moved from moderate- to low-stability class at increasing NaCl concentration. As far as P25-DOP and P25-PEG, they were always located within the moderate-stability class. Finally, at pH $\geq$ 8

(Fig. 5c), the functionalized P25-NPs dispersed in 1 mM NaCl were almost all classified as highly stable, except for the P25-PEG dispersions, again categorized as moderate stable.

In summary, at strong acid pH (2-4) the colloidal stability of the P25-NPs dispersions appeared to be functional group-dependent, while from pH 6 to 10 the colloidal stability seemed to be electrolyte concentration-dependent. A comparison among the different functional groups revealed that P25-COOH and P25-PEG dispersions were always located in the high- and moderate-stability class respectively, regardless of the pH and NaCl concentrations.

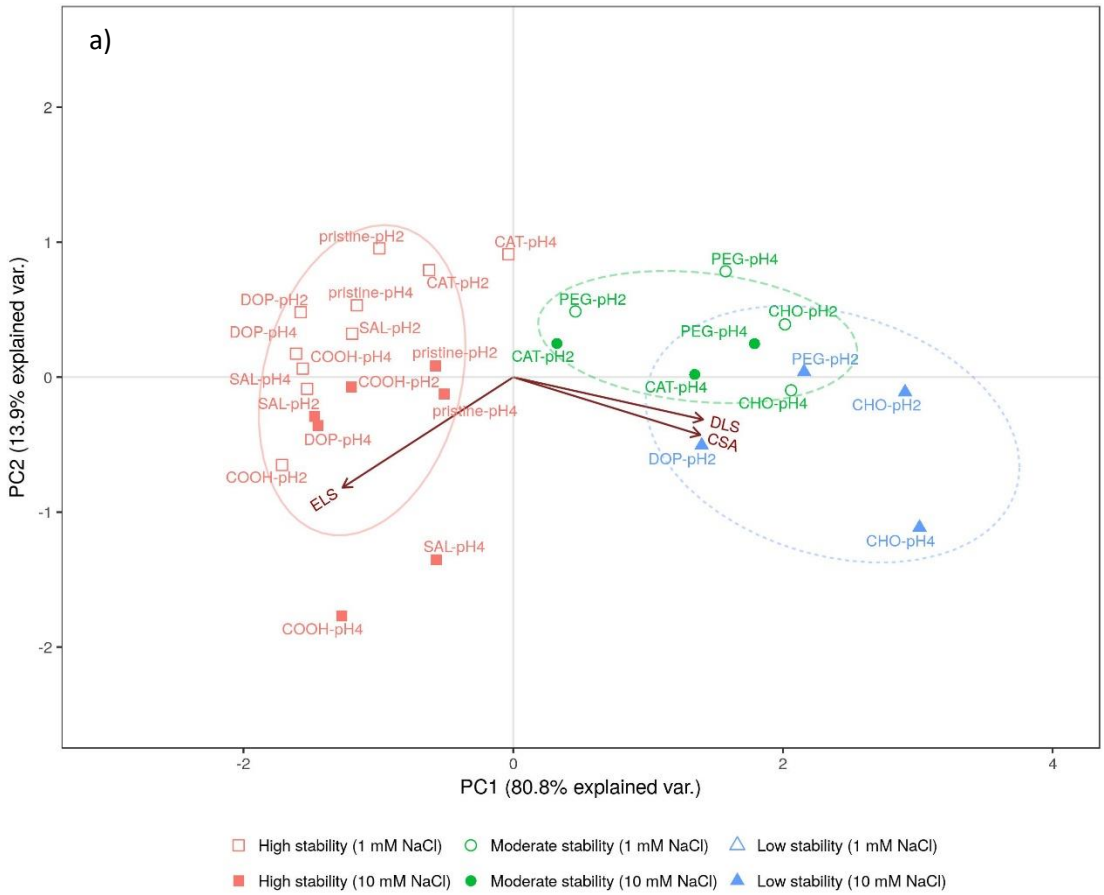

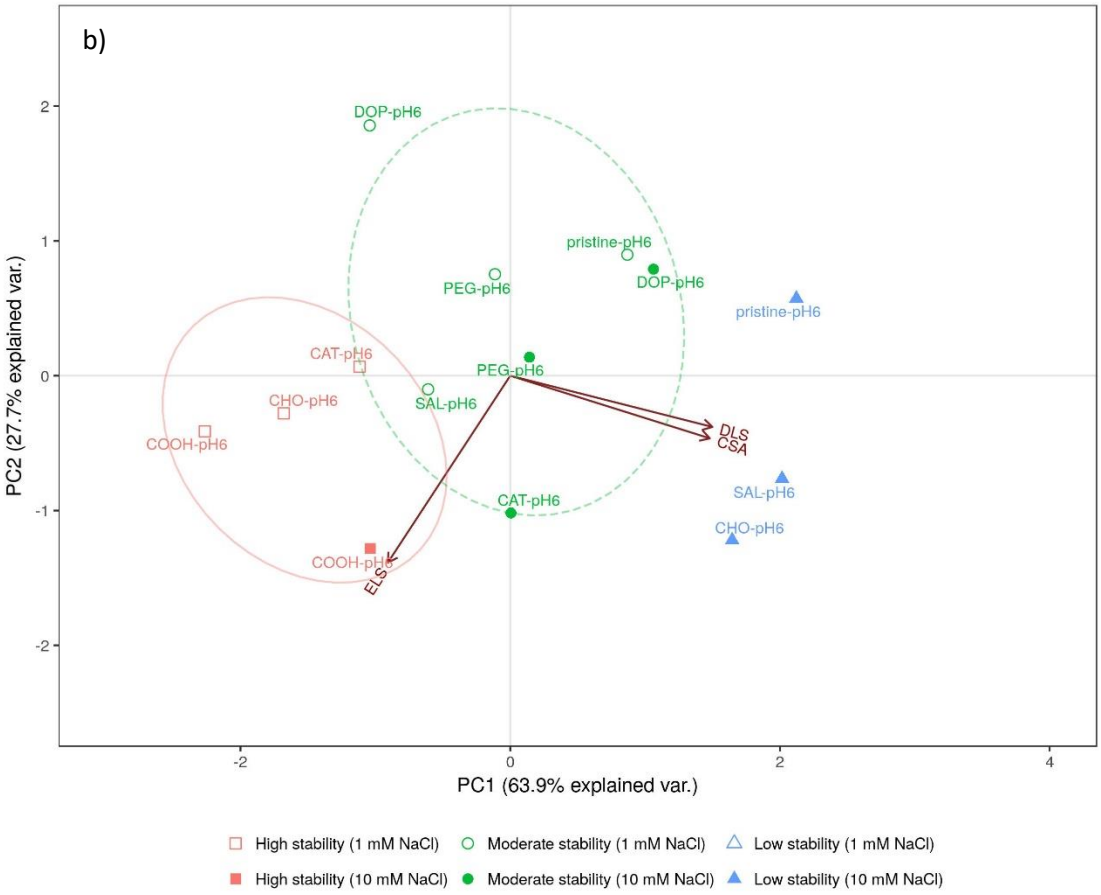
b)
DOP-pH6
pristine-pH6
PEG-pH6
DOP-pH6
pristine-pH6
CAT-pH6
PEG-pH6
CHO-pH6
SAL-pH6
COOH-pH6
DLS
CSA
SAL-pH6
CAT-pH6
CHO-pH6
COOH-pH6
ELS
PC2 (27.7% explained var.)
PC1 (63.9% explained var.)
High stability (1 mM NaCl)
Moderate stability (1 mM NaCl)
Low stability (1 mM NaCl)
High stability (10 mM NaCl)
Moderate stability (10 mM NaCl)
Low stability (10 mM NaCl)

425

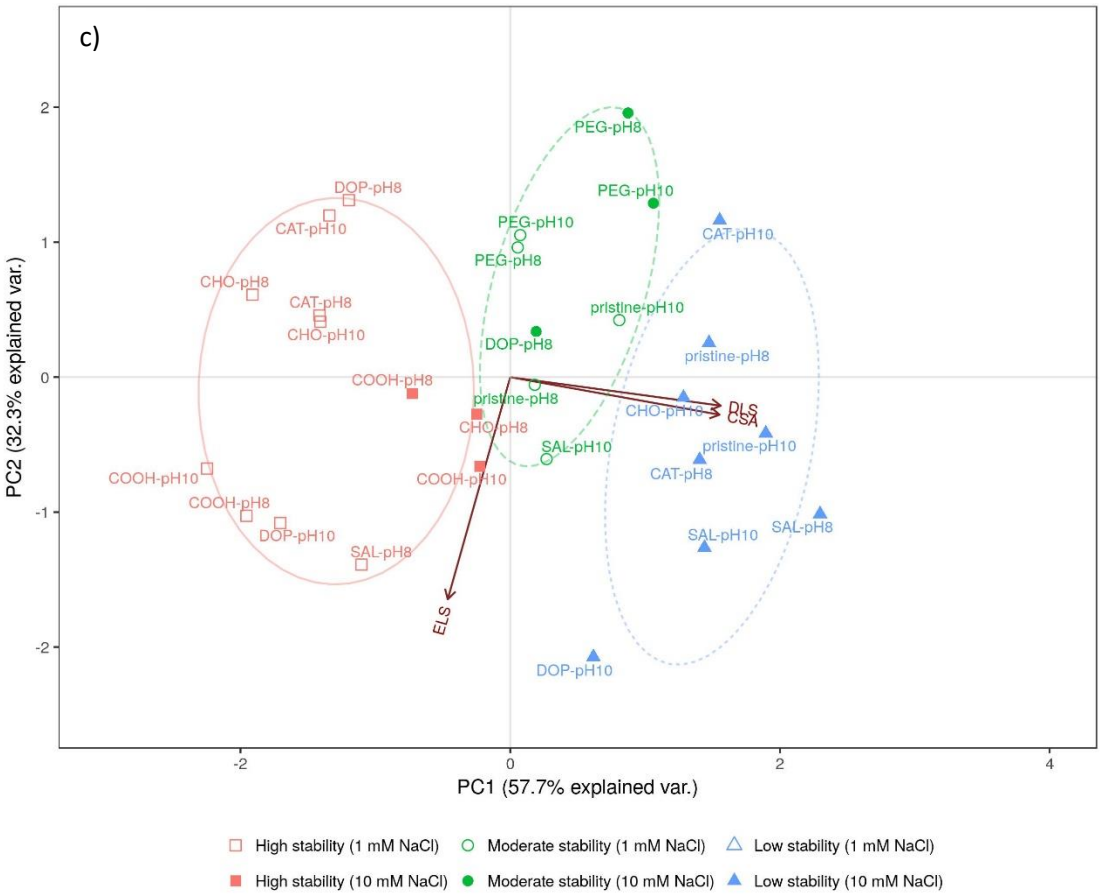
c)
PEG-pH8
DOP-pH8
PEG-pH10
CAT-pH10
PEG-pH10
PEG-pH8
CHO-pH8
CAT-pH8
pristine-pH10
CHO-pH10
DOP-pH8
pristine-pH8
COOH-pH8
pristine-pH8
CHO-pH8
CHO-pH10
DLS
CSA
SAL-pH10
pristine-pH10
COOH-pH10
COOH-pH10
CAT-pH8
COOH-pH8
SAL-pH10
SAL-pH8
DOP-pH10
SAL-pH8
ELS
DOP-pH10
PC2 (32.3% explained var.)
PC1 (57.7% explained var.)
High stability (1 mM NaCl)
Moderate stability (1 mM NaCl)
Low stability (1 mM NaCl)
High stability (10 mM NaCl)
Moderate stability (10 mM NaCl)
Low stability (10 mM NaCl)

426

Figure 5. PCA plots of the P25 NPs dispersed in 1 and 10 mM NaCl at different pH: a) 2 and 4, b) pH 6, c) 8 and 10. The ellipses represent a 68% confidence interval for experimental data, highlighting the regions corresponding to high, moderate, and low stability. For clarity, only the functional group of P25 functionalized NPs was reported in PCA labels.

3.3. Colloidal stability assessment as a function of dispersion media

The results obtained so far have highlighted the role of the different organic ligands in the colloidal stabilization of functionalized NPs dispersed in simple electrolyte solutions. The study was further extended to deionized water and ecotoxicological media i.e. AFW and AMW, to investigate how media characteristics (such as ionic strength and ionic composition) can affect the colloidal stability of the NPs dispersions, with respect to pristine P25. The results from DLS and CSA techniques are summarized in Table S6, showing a decrease of hydrodynamic diameter and sedimentation velocity in AFW and AMW for almost all the functionalized P25 NPs with respect to pristine. ELS data were not reported because of the difficulty to measure zeta-potential values in DW and ecotoxicological media (measurements prevented by the lack or too high concentration of electrolytes in solution).
For this reason, before applying the same statistical approach to the new dataset, consensus clustering analysis was applied only to DLS and CSA data and the results from the statistical analysis considering 3 vs 2 techniques were compared and summarized in Table S7. The comparison highlighted that >88% of samples (62 out of 70, which corresponds to an ARI of 0.67) were included in the same stability class, suggesting the possibility of using the same statistical approach, considering only two descriptors (DLS and CSA results). As a result, the stability classes of data obtained by dispersing P25 NPs in DW, AFW and AMW, were predicted starting from NaCl data, using a Nearest Neighbour classifier. Categorization of samples dispersed in DW at original pH as well as in 1 mM NaCl, 10 mM NaCl, AFW and AMW at pH 8 was graphically represented by PCA (Fig. 6). As expected, PCA in Fig. 6 highlighted that NPs dispersed in DW were all located in the highest stability class (very low agglomeration and sedimentation of NPs due to the absence of salts) while the ecotoxicological media composition (high salt concentration and presence of divalent cations) increased the destabilization of the dispersions, regardless the functional group on the NPs surface, locating all the data into the low stability class. However, as shown by the position of pristine in AFW and AMW from the PCA plot (i.e. outside from the ellipses), an increase of the colloidal stability of P25 NPs has been obtained because of the surface functionalization performed.

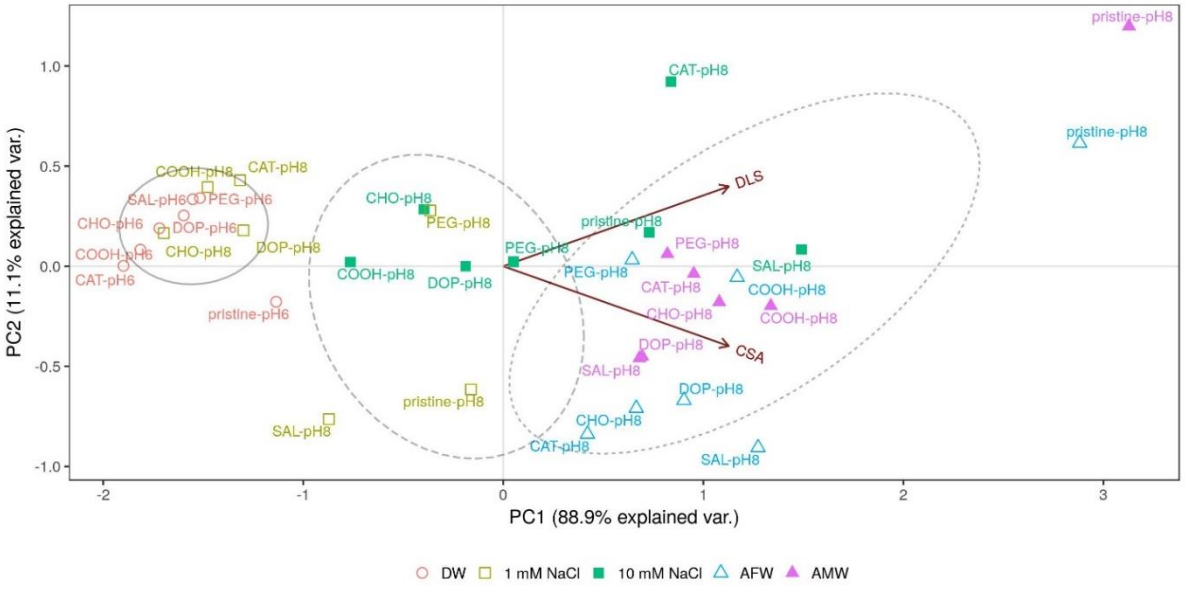

Figure 6. Hydrodynamic diameter ($d_{z\text{-}ave}$) and sedimentation velocity (Sed V) of pristine and functionalized NPs dispersed in Deionized Water (DW) at pH 6 and in 1 and 10 mM NaCl solutions, Artificial Fresh Water (AFW) and Artificial Marine Water (AMW), all at pH 8.

4. Conclusions

The work herein presented is one of the first studies employing multivariate statistical analysis methods to categorize experimental data of NPs dispersions into relative stability classes. The study highlighted that even small modifications of the NPs' surfaces can affect their colloidal stability towards the investigated parameters (i.e. dispersion media composition, pH, and electrolyte concentration). The performed statistical analyses helped to derive conclusions on the relationships of these extrinsic characteristics with the intrinsic properties of the modified nanomaterials (e.g. surface modification), which can support *in silico* and materials modelling to develop SbD strategies for TiO_2. In addition, the stability classification itself can directly inform the selection of dispersions/formulations for such strategies as well as for developing standard nano(eco)toxicological experiments for regulatory risk assessment.

Conflict of interest statement

We declare that we have no financial and personal relationships with other people or organizations that can inappropriately influence our work, there is no professional or other personal interest of any nature or kind in any product, service or company that could be construed as influencing the position presented in, or the review of, the manuscript entitled.

Acknowledgements

The authors are grateful to the European Commission for funding SUN project (FP7-NMP-2013-LARGE-7, Grant Agreement N° 604305), NanoFASE project (H2020-NMP-28-2014, Grant Agreement N° 646002), NanoRestART project (H2020-NMP-21-2014, Grant Agreement N° 646063), GRACIOUS project (H2020-NMP-28-2017, Grant Agreement N° 760840), NanoRestART project and CMCC Foundation for additional support.

Appendix A. Supplementary data

Supplementary data to this article can be found online

References

1 F. Piccinno, F. Gottschalk, S. Seeger and B. Nowack, *J. Nanoparticle Res.*, 2012, **14**, 1109.

2 J. E. Hutchison, *ACS Sustain. Chem. Eng.*, 2016, **4**, 5907–5914.

3 V. K. Sharma, K. M. Siskova, R. Zboril and J. L. Gardea-Torresdey, *Adv. Colloid Interface Sci.*, 2014, **204**, 15–34.

4 S. Ortelli, A. L. Costa, M. Blosi, A. Brunelli, E. Badetti, A. Bonetto, D. Hristozov and A. Marcomini, *Environ. Sci. Nano*, 2017, **4**, 1264–1272.

5 L. Canesi and I. Corsi, *Sci. Total Environ.*, 2016, **565**, 933–940.

6 J. H. E. Arts, M.-A. Irfan, A. M. Keene, R. Kreiling, D. Lyon, M. Maier, K. Michel, N. Neubauer, T. Petry, U. G. Sauer, D. Warheit, K. Wiench, W. Wohlleben and R. Landsiedel, *Regul. Toxicol. Pharmacol.*, 2016, **76**, 234–261.

7 D. M. Mitrano, S. Motellier, S. Clavaguera and B. Nowack, *Environ. Int.*, 2015, **77**, 132–147.

8 R. H. Gonçalves, W. H. Schreiner and E. R. Leite, *Langmuir*, 2010, **26**, 11657–11662.

9 T. D. Savić, M. I. Čomor, J. M. Nedeljković, D. . Veljković, S. D. Zarić, V. M. Rakić and I. A. Janković, *Phys. Chem. Chem. Phys.*, 2014, **16**, 20796–20805.

10 N. Kobayashi and R. Arai, *Curr. Opin. Biotechnol.*, 2017, **46**, 57–65.

11 A. Burger, R. D. Costa, V. Lobaz, W. Peukert, D. M. Guldi and A. Hirsch, *Chem. - A Eur. J.*, 2015, **21**, 5041–5054.

12 Q. Wei, T. Becherer, P.-L. M. Noeske, I. Grunwald and R. Haag, *Adv. Mater.*, 2014, **26**, 2688–2693.

13 D. Selli and C. Di Valentin, *J. Phys. Chem. C*, 2016, **120**, 29190–29201.

14 C. M. Bishop, *Pattern Recognition and Machine Learning (Information Science and Statistics)*, Springer-Verlag New York, Inc. Secaucus, NJ, USA, 2006.

15 C. M. Sayes, P. Alex Smith and I. V. Ivanov, *Int. J. Nanomedicine*, 2013, **8**, 45–56.

16 X. Z. Wang, Y. Yang, R. Li, C. Mcguinnes, J. Adamson, I. L. Megson and K. Donaldson, *Nanotoxicology*, 2014, **8**, 465–476.

17 R. Tantra, S. Jing, S. K. Pichaimuthu, N. Walker, J. Noble and V. A. Hackley, *J. Nanoparticle Res.*, 2011, **13**, 3765–3780.

18 OECD Guidelines for Testing of Chemicals N° 203 - Fish Acute Toxicity Test (Annex 2 Composition of the recommended reconstituted water), 1992, 1–9.

19 ASTM D1141-98 (Reapproved 2003). Standard Practice for the Preparation of Substitute Ocean Water, 2003.

20 J. S. Taurozzi, V. A. Hackley and M. R. Wiesner, *Nanotoxicology*, 2011, **5**, 711–729.

21 J. S. Taurozzi and V. A. Hackley, *Preparation of Nanoparticle Dispersions from Powdered Material Using Ultrasonic Disruption*, 2012.

22 K. Suttiponparnit, J. Jiang, M. Sahu, S. Suvachittanont, T. Charinpanitkul and P. Biswas, *Nanoscale Res. Lett.*, 2011, **6**, 27.

23 Y. Zhang, Y. Chen, P. Westerhoff, K. Hristovski and J. C. Crittenden, *Water Res.*, 2008, **42**, 2204–2212.

24 S. Bhattacharjee, *J. Control. Release*, 2016, **235**, 337–351.

25 K.-M. Kim, H. M. Kim, W.-J. Lee, C.-W. Lee, T. Kim, J.-K. Lee, J. Jeong, S.-M. Paek and J.-M. Oh, *Int. J. Nanomedicine*, 2014, **9**, 29–40.

26 T. C. A. Almeida, A. L. Larentis and H. C. Ã. Ferraz, *PLoS One*, 2015, **10**, 1–18.

27 A. Brunelli, A. Zabeo, E. Semenzin, D. Hristozov and A. Marcomini, *J. Nanoparticle Res.*, 2016, **18**, 113.

28 D. Lerche, *J. Dispers. Sci. Technol.*, 2002, **23**, 699–709.

29 R Core Team, 2016.

30 D. Meyer, E. Dimitriadou, K. Hornik, A. Weingessel and F. Leisch, 2015.

31 W. N. Venables and B. D. Ripley, *Modern Applied Statistics with S*, Springer Publishing Company, 2010.

32 F. Saeed, N. Salim and A. Abdo, *J. Cheminform.*, 2012, **4**, 37.

33 L. Hubert and P. Arabie, *J. Classif.*, 1985, **2**, 193–218.

34 G. W. Milligan and M. C. Cooper, *Multivariate Behav. Res.*, 1986, **21**, 441–458.

35 J. M. Santos and M. Embrechts, eds. C. Alippi, M. Polycarpou, C. Panayiotou and G. Ellinas,

Springer Berlin Heidelberg, Berlin, Heidelberg, 2009, pp. 175–184.
36 Y. Kakuma, A. Y. Nosaka and Y. Nosaka, *Phys. Chem. Chem. Phys.*, 2015, **17**, 18691–18698.
37 I. A. Janković, Z. V. Šaponjić, M. I. Čomor and J. M. Nedeljkovic, *J. Phys. Chem. C*, 2009, **113**, 12645–12652.
38 A. León, P. Reuquen, C. Garín, R. Segura, P. Vargas, P. Zapata and P. A. Orihuela, *Appl. Sci.*, 2017, **7**, 49.
39 S. V. Manorama, K. Madhusudan Reddy, C. V. Gopal Reddy, S. Narayanan, P. Rajesh Raja and P. R. Chatterji, *J. Phys. Chem. Solids*, 2001, **63**, 135–143.
40 M. Kosmulski, *J. Colloid Interface Sci.*, 2009, **337**, 439–448.
41 A. Praetorius, J. Labille, M. Scheringer, A. Thill, K. Hungerbühler and J.-Y. Bottero, *Environ. Sci. Technol.*, 2014, **48**, 10690–10698.
42 N. Mandzy, E. Grulke and T. Druffel, *Powder Technol.*, 2005, **160**, 121–126.
43 F. Loosli, P. Le Coustumer and S. Stoll, *Water Res.*, 2013, **47**, 6052–6063.